Influence of the Internal Energy Model on DSMC Flow Results for Rarefied Spacecraft Plumes

Jason A. Cline

Spectral Sciences Inc., 4 Fourth Ave., Burlington, MA, 01803

INTRODUCTION

In low Earth orbit, energetic collisions between molecules from spacecraft emissions and atmosphere are observed to produce a luminescent interaction layer [1]. These collisions deposit a substantial amount of energy into the internal modes of the molecules. The rate at which this energy is deposited and the distribution of that energy among translational, rotational, and vibrational degrees of freedom govern many properties of the interaction layer, including its temperature distribution, shape, and spectral radiance.

Direct simulation Monte Carlo (DSMC) models [2] are among the important tools for predicting the interactions between the atmosphere and spacecraft surfaces or gases emitted by spacecraft in low Earth orbit [3, 4]. Recent experimentally-determined vibrational transition chemistry (such as for O + CO [5]) now enables use of an internal energy model with explicit transition cross-sections between ground and explicitly-enumerated quantized excited vibrational states which we will explore in this work. The SOCRATES[1] and SOCRATES-P[2] codes [6, 7] are DSMC codes that are specialized for computing spacecraft contamination flow fields [8], radiative byproducts of space vehicle effluents and exhausts [9–11] and their spectra, and for use in analysis of molecular beams [12, 13]. The SOCRATES code was originally developed in the 1980s and uses computationally economic approaches such as a variable hard-spheres (VHS) interaction model [14] with a single global ω parameter, a global constant probability for inelastic collisions, and a single per-species constant for the number of internal degrees of freedom. The parallel version of the code has several additional models for total cross sections and energy redistribution. Despite the apparent simplicity of the original models in SOCRATES, they are highly successful in their primary applications. In this work we use DSMC calculations in a simplified geometry to explore the sensitivity of flow results to the internal energy models by comparing flows computed using several internal energy and energy transfer schema, including a model with detailed quantized vibrational transitions.

MODELS

Several models are pertinent to the transfer of internal energy, including the cross-section model, the internal energy models in each species, and energy redistribution algorithms. We begin with the different internal degrees of freedom among which energy is redistributed during a collision.

Translational degrees of freedom are governed by the cross-section model. For this work, the sole potential model is the variable hard spheres (VHS) model [14], that allows the effective cross-section of a molecule to vary with collision velocity through a power-law relation, $d = d_{\mathrm{ref}} \left(c_{r,\mathrm{ref}}/c_r\right)^{(\omega-1/2)}$. The ω exponent is significant to internal energy redistribution because there are $(5-2\omega)$ translational degrees of freedom in a collision involving two VHS

[1] Spacecraft/Orbiter Contamination Representation Accounting for Transiently Emitted Species
[2] SOCRATES, parallel version

molecules. The VHS parameters are set using viscosity data [15] according to the methods of Bird [2], sec. 3.5 and 4.3.

The next category of degrees of freedom is for molecular internal energy. The simplest internal energy model is a lumped constant model. In this model, all non-translational internal energy (rotational, vibrational, and electronic) is lumped into ζ internal degrees of freedom, such that on average, $E_i = (\zeta/2)kT_i$ and ζ is constant. ζ relates directly to heat capacity C_p through $\zeta = (2C_p/k) - 5$. This is not to suggest that C_p data could be used outright to assign ζ, but rather that C_p gives $\langle\zeta\rangle$ where the ensemble is considered is one in equilibrium with the temperature of the tabulated C_p. Consider the CO molecule as described in the high-temperature thermodynamic database of McBride and Gordon [15]. At low temperature CO has a ζ of 2.0, but approaching Θ_v, ζ increases to 4.0. As the energy regime of our calculation is commensurately high, we will examine each of these values.

In a collision, the Larsen-Borgnakke [16] method is used to assign energy to every degree of freedom in the collision complex. The method, however, says nothing about the mechanism for or the rate at which these processes occur—only the outcome. The rate is governed by an externally assigned conditional probability that, given a collision occurs, it is inelastic. This conditional probability, or fraction of collisions that are inelastic (f_i) has in the past been set arbitrarily to 50% for lack of better information. Higher-fidelity treatments for the vibrational and rotational collision number [17–19] may be beneficial because they add a local collisional energy dependence to the collision number. The focus of this study, in the area of energy transfer rate, is limited however to comparing a global constant fraction of inelastic collisions with the chemical-reaction based vibrational transfer kinetics.

Explicit Models for Vibrational Exchange Kinetics

When explicit information regarding a certain type of energy transfer is available, it is preferable to use it instead of the Larsen-Borgnakke and collision-number methods for that particular degree of freedom. One way to model vibrational energy transfer is to treat vibrational transitions as explicit chemical reactions. Under this methodology, vibrational degrees of freedom are treated explicitly and separately. For example, in a lumped internal-energy model of CO that usually has $\zeta = 4.0$, it would instead remain with $\zeta = 2.0$; explicitly excited species $\{\mathrm{CO}(v)\}$ such that $v > 0$ are added explicitly through a chemical reaction model. Now, at the cost of complexity, we have control of the energy dependent rates of the vibrational transitions.

Chemical reaction rate constants are generally parameterized in the Arrhenius form.

$$k = AT^n \exp(E_a/kT) \tag{1}$$

These rate constants are measured in equilibrium gas, with a distribution of collision velocities. For use in DSMC, the reaction is Laplace-inverse transformed [14] to yield the following cross-section:

$$v_r\sigma_r = \sqrt{\pi}(1+\delta_{ij})A\sqrt{1-E_a/E_c}\,(E_c-E_a)^n/(2k^n\Gamma(n+1.5)) \tag{2}$$

where v_r is the relative velocity of the collision pair, σ_r is the reactive cross-section, δ_{ij} is one if the colliding molecules are the same species and zero otherwise, and E_c is the translational collision energy. Given that a pair of species collide, the probability of reaction is $\sigma_r/\sigma_{\mathrm{VHS}}$.

Two mechanisms are considered: a *two-state mechanism* and a *multi-state mechanism*. Although we include the radiative chemistry here, we will turn it off for some of the calculations to separate out its influence. The two-state mechanism involves ground and excited CO as shown in Table 2. The two-state model uses an excitation cross-section fitted to the data of Braunstein and Duff [20], wherein $A = 2.81\times10^{-25}\ \mathrm{m^3s^{-1}K^{-}}^n$, $n = 2.2$, and $E_a = 4.25\times10^{-20}$ J. For the reverse reaction, the same A and n is used, but the activation energy (E_a) is assigned to zero.

The multistate mechanism involves several reactions, as shown in Table 3, where in the excitation reaction, v' may be much higher than the original v state. The preceding mechanisms are treated as independent of the J state. For the multistate model, only the reactive cross sections of Figure 6a in Brunsvold et al. [5] were used. Brunsvold et al. separately determined the cross sections for vibrational excitation due to reaction (O substitution) and to inelastic collisions. Using the cross-sections for the reactive channels only was a simplification for convenience, based on the finding of Brunsvold et al. that the reactive and inelastic vibrational excitation cross-sections were comparable. The simplification will lead to underestimating the incidence of vibrational excitations perhaps by a factor of two.

In this context, the relevant difference between the two-state and the multi-state mechanisms is that in the two-state mechanism limits the amount of energy deposited into the vibrational mode to one quantum, whereas the multistate model allows multiple quanta.

CALCULATIONS

Our calculations involve a highly-simplified system in which there are two translationally-cold flows impinging at right angles. This is analogous to a crossed molecular beam experiment or a thruster firing at 90° to the travel direction. Figure 1 shows the flow schematically. All four boundary conditions are *vacuum* boundaries—molecules that cross the boundary are removed from the simulation. Flow is introduced from the left and bottom boundaries. Though decidedly imperfect, this geometry is a convenient tool for qualitatively surveying the sensitivity of the scattering behavior to the different internal energy transfer and internal energy models.

In the preceding section, we identified several parameters that might affect the shape of a flow feature: ω, ζ, f_i (the fraction of collisions that are inelastic), and explicit vibrational kinetics. We survey these conditions using the system of atomic oxygen (O) and carbon monoxide (CO) at a center-of-mass relative velocity of 8000 m/s. Table 1 shows the conditions explored in this survey. The nominal conditions, with label "N," are for $\omega = 0.75$, $\zeta = 2.0$, $f_i = 0.5$, and no radiation or explicit vibrational energy transfer. This condition best corresponds to a low-energy CO collision.

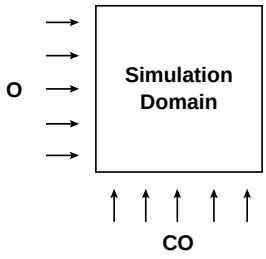

FIGURE 1. Schematic of simplified cross-flow calculation.

All calculations were performed in 2D planar symmetry on a 100×100 grid of square 15 m DSMC cells. The DSMC time step is 4×10^{-4} s, the ratio of real to simulated particles is 10^{17}, and the total number of simulated particles was approximately 1.3×10^{6}. Both O and CO flow into the cell at 5656 m/s from the left and bottom, respectively, at a translational temperature of 4 K and a density of 2×10^{16} molecules per m^3. The calculations were allowed 4000 DSMC steps to come to steady state, after which another 4000 steps were used for sampling. Each case used 8 AMD Athlon CPUs and ran for roughly 60 minutes. In most cases (N, and A–E) there is no chemistry. In the remainder of the cases, vibrational transitions are treated as chemical reactions using the chemical mechanism described previously. True chemical-change reactions, such as of O+O to yield O_2 and O+CO to yield CO_2, were neglected.

Influence of the Inelastic Fraction

The first parameter examined is f_i, the fraction of collisions that are inelastic. Figures 3 and 4 show the translational temperature and the number density, respectively, of the flow fields for inelastic fractions f_i of 0.0, 0.1, and 0.5. The higher values of f_i, 0.5 and 1.0, have virtually identical results in both temperature and density, suggesting that at f_i=0.5 the internal modes of the molecules have already equilibrated with their local translational environment. At f_i of 0, a condition equivalent to CO behaving as a monatomic gas, the flowfield is different than for $f_i \geq 0.5$. The most pronounced effect is seen in the overall translational temperature: the CO that cannot transfer energy into its internal modes deposits it into translation, resulting in a higher-temperature (14 000 K) contour along the CO side of the interaction zone than in the other cases (10 000–12 000 K). The shape of the density peak is also affected. At $f_i = 0.1$ the results appear intermediate to those at f_i=0.0 and 0.5. The composition of the flow in all runs is relatively constant, with a typical pattern shown in Figure 2.

This result is consistent with our general expectation that the rotational temperature is often in equilibrium with its

TABLE 1. Matrix of parameters surveyed for the system O+CO. Off-nominal parameters are bold-typeset for emphasis.

Label	ω	ζ	f_i	Explicit Vibrations	Radiative
N	0.75	2.0	0.5	none	no
A	0.75	2.0	**0.0**	none	no
B	0.75	2.0	**0.1**	none	no
C	0.75	2.0	**1.0**	none	no
D	0.75	**4.0**	0.5	none	no
E	**0.90**	2.0	0.5	none	no
F	0.75	2.0	0.5	**two-state**	no
G	0.75	2.0	0.5	**multistate**	no
H	0.75	2.0	0.5	**two-state**	**yes**
J	0.75	2.0	0.5	**multistate**	**yes**

TABLE 2. Two-state equation set.

$$\begin{aligned} \mathrm{CO} + \mathrm{M} &\leftrightarrows \mathrm{CO}(*) + \mathrm{M} \\ \mathrm{CO}(*) &\rightarrow \mathrm{CO} + \text{ photon} \end{aligned}$$

TABLE 3. Multi-state equation set.

$$\begin{aligned} \mathrm{CO}(v) + \mathrm{M} &\leftrightarrows \mathrm{CO}(v') + \mathrm{M} \\ \mathrm{CO}(v' = v+1) &\rightarrow \mathrm{CO}(v) + \text{ photon} \end{aligned}$$

In the excitation reaction, v' may be much higher than v.

local environment. It also shows that, in this regime, the results are not sensitive to the value of f_i. On the other hand, when vibrational degrees of freedom are lumped in with the rotational degrees of freedom, an inconsistency could develop.

Influence of the Viscosity Exponent

The second parameter examined is the viscosity exponent ω, which was increased from 0.75 to 0.90. Figure 5, shows the temperature, number density, and CO rotational temperature, respectively, in the flowfield at ω values of 0.75 and 0.90. The largest effect is in the density, where the peak density region becomes smaller and more symmetrical for the ω=0.90 case. The differences in terms of translational and rotational temperature are small. The ω=0.90 case has a lower overall rotational temperature, but appears to have more evenly-distributed translational temperature.

What is interesting here is that there is a similarity in the morphology of the interaction region for ω=0.90 and that at ω=0.75 with f_i of 0.1 and 0.5. The data suggest that an intermediate value of f_i may have the same effect on interaction layer shape as a change in ω. Although variation in ω has been previously shown to change the plume shape [9], the effect of f_i has not been recently investigated in a radiation context.

Influence of the Internal DOF

The next examination compares CO frozen in the ground state (ζ=2.0) with vibrationally-excitable CO with several kinds of models: a ζ=4.0 CO molecule, a ζ=2.0 CO molecule with a two-state vibrational chemistry model, and a ζ=2.0 CO molecule with a multi-state vibrational chemistry model. Figures 6 and 7 show the number density and CO rotational temperature, respectively, for these four cases. Adding the vibrational DOF produces a denser CO-O interaction layer, although the flow for the two-state model is not as dense as that of the multistate model and the ζ=4.0 model. The multistate model and the ζ=4.0 model show densities that are 10% higher than for the two-state model, and 20% higher than the vibrationally frozen case. As one might expect from the increased density, the translational temperatures (not shown) are accordingly lower. On the other hand, the rotational temperature of CO is cooler than nominal in the ζ=4.0 case, but much warmer in the two-state and multistate cases, with the two-state case showing the highest rotational temperatures.

Influence of Radiation

To include radiation, the first-order decay reaction of CO at $v = 1$ through $v = 10$ were included in the calculation. We used the Einstein A values for $J \approx 90$ from Figure 4 of Braunstein and Duff [21] for the multistate model and arbitrarily assigned a rough mean A of 60 s^{-1} for the two-state model.

In the previous section we saw the different effects of a two-state and a multistate model for excitation. The addition of radiation does not make a large difference in this scenario. The general trend is to reduce the flow field temperature (Figure 8); this was more prominent in the two-state model than in the multistate model. There was little observable change in the density. There was also little observable change in the CO rotational temperature.

SUMMARY AND FUTURE WORK

In this work the sensitivity of the spatial maps of density and temperature are assessed in terms of the VHS ω parameter, the fraction of inelastic collisions f_i, and the model for the internal state of the molecule through changes in ζ or through explicit chemical reactions. Comparing the nominal case with the cases with explicit vibrational chemistry, we find that turning off a reaction set (such as might be done when exploring kinetic mechanism) can significantly influence the peak translational temperature and the rotational temperature distribution in the flow field. Additionally, there is evidence to suggest a covariance between the ω parameter and the f_i in influencing the morphology of the interaction layer. Absent was the α parameter in the variable soft spheres [22] potential, which may also affect plume shape, and the survey of different collision number techniques that can effectively assign f_i as a function of local conditions, which is relegated to future work.

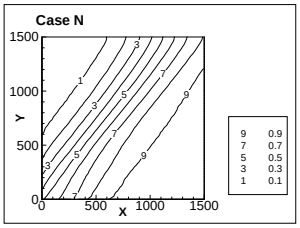

FIGURE 2. CO mole fraction field at f_i values of 0.5 (typical).

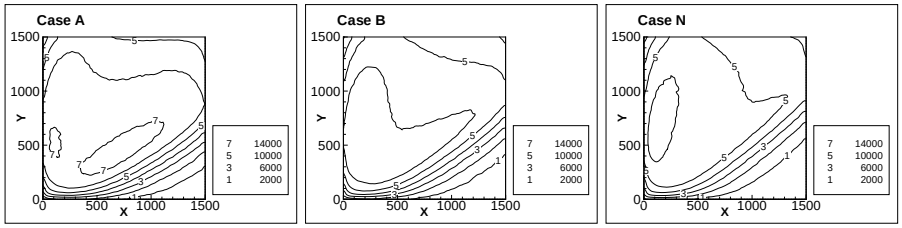

FIGURE 3. Overall translational temperature (K) fields at f_i values of 0.0, 0.1, and 0.5.

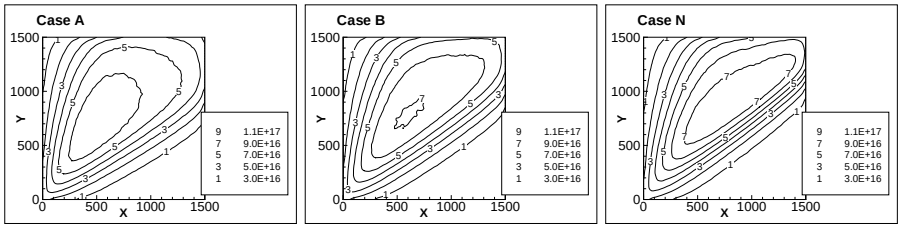

FIGURE 4. Total number density (m^{-3}) fields at f_i values of 0.0, 0.1, and 0.5.

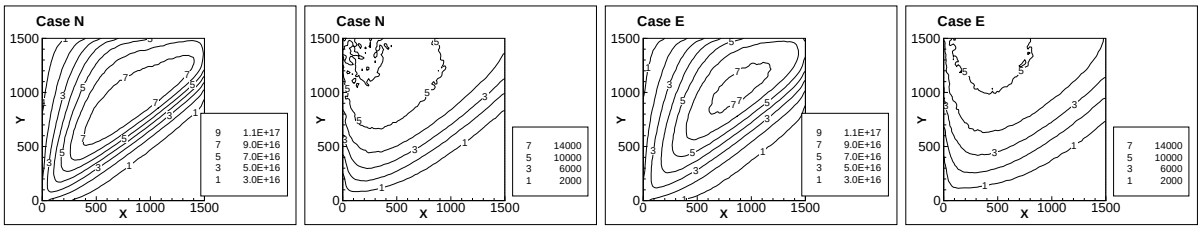

FIGURE 5. From left to right: overall translational temperature (K), total number density (m^{-3}), and CO rotational temperature (K) fields at ω values of 0.75 and 0.90. The top row corresponds to ω of 0.75; the bottom is ω of 0.90.

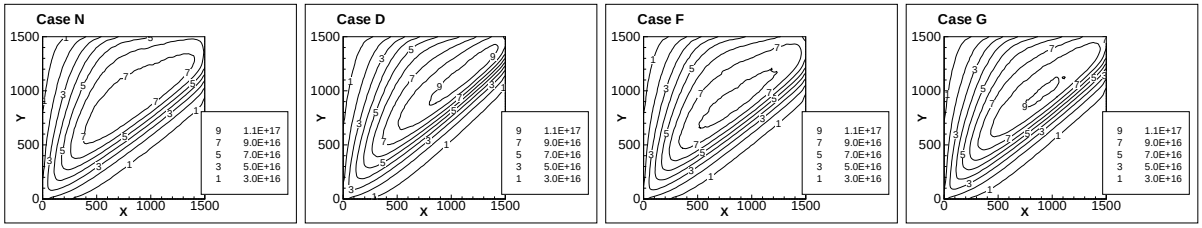

FIGURE 6. Total number density (m^{-3}) fields. The cases are for ζ=2.0, ζ=4.0, ζ=2.0 with a two-state vibrational model, and ζ=2.0 with a multistate vibrational model.

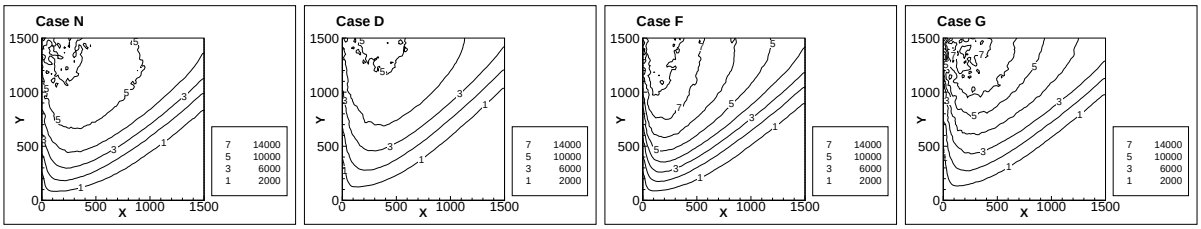

FIGURE 7. CO rotational temperature (K) fields. The cases are for ζ=2.0, ζ=4.0, ζ=2.0 with a two-state vibrational model, and ζ=2.0 with a multistate vibrational model.

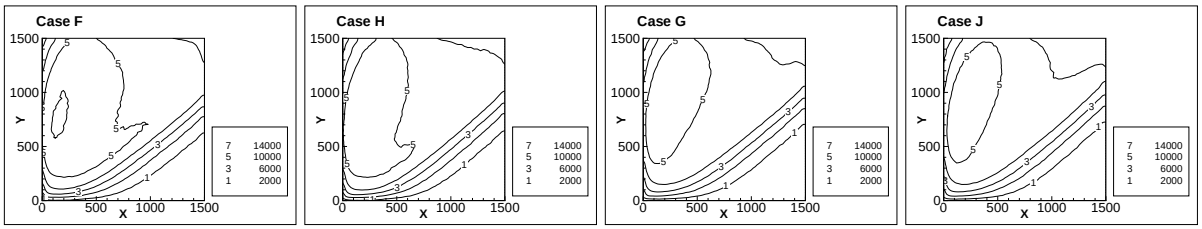

FIGURE 8. Overall translational temperature (K) fields. The left two frames are the non-radiative and radiative results for the two-state model, respectively. The right two frames are the non-radiative and radiative results for the multi-state model, respectively. See nominal Case N (no vibrations) in Figure 5 for comparison.

ACKNOWLEDGMENTS

The author acknowledges several helpful discussions with Sergey Gimelshein of the University of Southern California and with Matthew Braunstein and Larry Bernstein of Spectral Sciences, and with Bill Dimpfl of The Aerospace Corporation. The DSMC code SOCRATES-P, used for this study, was developed under sponsorship from the Air Force Research Laboratory, the United States Department of Defense High Performance Computing Modernization Office, and the Missile Defense Agency under contracts F19628-00-C-0006 and FA8718-05-C-0077. The author thanks Spectral Sciences for internal R&D funding to perform this work.

REFERENCES

1. B. L. Upschulte, and G. E. Caledonia, *J. Chem. Phys.* **96**, 2025–33 (1992).
2. G. A. Bird, *Molecular Gas Dynamics and the Direct Simulation of Gas Flows*, Clarendon Press, Oxford, 1994.
3. B. D. Hester, Y. Hui Chiu, J. R. Winick, R. R. Dressler, L. S. Bernstein, M. Braunstein, and P. F. Sydney, *Journal of Spacecraft and Rockets* **46**, 679–688 (2009).
4. J. A. Cline, T. K. Minton, and M. Braunstein, *J. Spacecraft and Rockets* **42**, 810–816 (2005).
5. A. L. Brunsvold, H. P. Upadhyaya, R. C. J. Zhang, T. K. Minton, M. Braunstein, and J. W. Duff, *J. Phys. Chem. A* **112**, 2192–2205 (2008).
6. J. B. Elgin, and L. S. Bernstein, The theory behind the SOCRATES code, Tech. Rep. PL–TR–92–2207, Geophysics Directorate, Phillips Laboratory, Hanscom AFB, MA (1992).
7. M. Braunstein, Progress on parallelizing a general purpose direct simulation Monte Carlo (DSMC) code for high performance computing applications, Tech. Rep. 20030107284, NASA (2003), presented at the AMOS 2003 Technical Conference, Maui, HI.
8. M. Braunstein, "Chemical and Flowfield Modeling for Enhanced Analysis of Contamination Experiments," in *40th AIAA Aerospace Sciences Meeting*, Reno, NV, 2002, AIAA Paper 2002–0213.
9. W. L. Dimpfl, G. C. Light, and L. S. Bernstein, "Molecular Dynamics from Remote Observations of CO(a) from Space Shuttle Plumes," 2003, AIAA Paper 2003-6204.
10. L. S. Bernstein, J. B. Elgin, C. P. Pike, D. J. Knecht, E. Murad, T. F. Zehnpfennig, G. E. Galica, and A. T. Stair, *J. Geophys. Res.* **101**, 383 (1996).
11. R. A. Viereck, E. Murad, C. P. Pike, S. B. Mende, G. A. Swenson, J. B. Elgin, L. S. Bernstein, and S. Lucid, *J. Geophys. Res.* **100**, 5819 (1995).
12. M. Braunstein, A. L. Brunsvold, D. J. Garton, and T. K. Minton, *J. Chem. Phys.* **120**, 2238–46 (2004).
13. M. Braunstein, and I. J. Wysong, "Direct Simulation Monte Carlo Modeling of High Energy Chemistry in Molecular Beams: Chemistry Models and Flowfield Effects," in *22nd International Rare Gas Dynamics Conference*, Sydney, Australia, 2000.
14. G. A. Bird, *Progr. Astro. Aero.* **74**, 239–55 (1981).
15. B. J. McBride, and S. Gordon, Computer program for calculation of complex chemical equilibrium compositions and applications, Tech. Rep. NASA RP-1311, National Aeronautics and Space Administration, Lewis Research Center, Cleveland, OH (1996).
16. C. Borgnakke, and P. S. Larsen, *Journal of Computational Physics* **18**, 405 (1975).
17. Parker, *Phys. Fluids* **2**, 449 (1959).
18. I. D. Boyd, *J. Thermophysics* **4**, 478 (1990).
19. N. E. Gimelshein, S. F. Gimelshein, and D. A. Levin, *Phys. Fluids* **14**, 4452 (2002).
20. M. Braunstein, and J. W. Duff, *J. Chem. Phys.* **112**, 2736–2745 (2000).
21. M. Braunstein, and J. W. Duff, *Journal of Physical Chemistry A* **113**, 10795–802 (2009).
22. K. Koura, and H. Matsumoto, *Physics of Fluids A* **3**, 2459–2465 (1991).